From regular to chaotic motions through the work of Kolmogorov

Alessandra Celletti[1], Claude Froeschlé[2] and Elena Lega[3]

March 14, 2003

[1] Dipartimento di Matematica, Università di Roma "Tor Vergata", Via della Ricerca Scientifica, 00133 Roma, Italy, e–mail: celletti@mat.uniroma2.it
[2] Observatoire de Nice,
BP 229, F–06304 Nice Cedex 4 (France),
e–mail: claude@obs-nice.fr
[3] Observatoire de Nice,
BP 229, F–06304 Nice Cedex 4 (France),
e–mail: elena@obs-nice.fr

1 Introduction

We know that the solar system survived catastrophic events since 5 billion years, which corresponds to the estimated age of our star. Although the Sun will become a red giant in about 5 billion years and it will destroy the regularity of the planetary motions, the question of the stability of the solar system within this time interval remains open.

This problem has been faced since antiquity and it motivated the development of many studies in mathematical physics. In this context, the so–called *perturbation theory* was developed by Laplace, Leverrier, Delaunay and Lagrange, with the aim to investigate the dynamics of the planetary motion. To be more precise, let us start with the simplest model of planetary evolution, i.e. the two–body problem, consisting in the study of the motion of a planet under the gravitational influence of the Sun. As is well known, the solution is provided by Kepler's laws, which guarantee that (in this approximation) the planet orbits the Sun on an elliptic orbit, the Sun being located at one of the foci. The two–body problem is the typical example of an *integrable* system, since its solution can be explicitly provided. In order to get a more realistic model, we should include the gravitational attraction of the other bodies of the solar system. Therefore, let us start by considering the *three–body problem*, where the effect of a third body is included. Despite many efforts performed by a lot of scientists in the XIX century, a mathematical solution of this problem cannot be found: indeed, H. Poincaré proved the non–integrability of the three-body problem ([48]). However, if we consider that the action of the third body (whatever it is: planet, satellite or comet) is small compared to the force exerted by the Sun, we can include the three–body problem in the class of the *nearly–integrable* systems. In our example, the integrable approximation is provided by the two–body problem and the strength of the nonlinearity is relatively small (being proportional to the mass ratio of the primaries, i.e. the third body and the Sun). In this framework, perturbation theory provides useful tools to give (in particular cases) an approximate solution of the equations of motion. However, such theory does not allow to draw definite conclusions about the stability of the dynamics, since the mathematical series involved in the construction of the approximate solution are generally divergent.

It was only in the '50s that A.N. Kolmogorov made a major breakthrough in the study of nearly–integrable systems. He proved ([32]) that for slightly perturbed systems, under quite general assumptions, some regions of the phase space remain regular. We stress that Kolmogorov's theorem can be used in a constructive way to prove the stability of motions. A few years later, the pioneering work of Kolmogorov was extended by V.I. Arnold ([1]) and J. Moser ([44]), giving rise to the so-called KAM theory. Though the original estimates of the KAM theorem do not provide rigorous results in agreement with the physical predictions, recent implementations of computer-assisted proofs show that KAM theory can be efficiently used in model problems, yielding results in agreement with the experimental observations. KAM theory was the starting point for a broad investigation of the stability of nearly-integrable systems, which is briefly reviewed in §2. Moreover, it opened a new field of research, related to the development of numerical experiments.

In this framework, the simulations performed by M. Hénon and C. Heiles ([30]) filled the gap between theory and experiments, opening a bridge toward the understanding of the global study of the dynamical properties of the whole phase space. In particular, the concept of chaos makes its appearance in a wide range of physical problems. The extent of chaotic motions is provided by the computation of Lyapunov's exponents, which allow to measure the divergence of nearby trajectories. This concept was recently refined to investigate the behaviour of weakly chaotic motions, through the implementation of frequency analysis and Fast Lyapunov Indicators (hereafter, FLI). In §3 we review some applications of such methods to investigate the topology of the phase space. Moreover, the computation of the FLIs allowed to study the transition from Chirikov's to Nekhoroshev's regime and therefore it provides results about diffusion in Hamiltonian systems.

2 Stable motions

2.1 Integrable and non–integrable systems

When dealing with real physical problems, it is rather exceptional to find a mathematical solution which describes the dynamics of the system. If the solution cannot be found, the typical approach is to diminish the complexity of the problem by introducing a reasonable set of assumptions. If a solution of the most simplified model can be found, then one can proceed to reintroduce the ingredients which make the model closer to reality. However, such procedure can fail even at the basic step, when the simplest model is considered.

A familiar example of this approach is provided by the investigation of the stability of the solar system. The reality consists of 9 planets orbiting around the Sun, a lot of satellites moving about the planets, thousands of small objects like comets and asteroids. Moreover, one should take into account the oblateness of the solar system bodies, the existence of rings around the major planets, tides, solar wind effects and so on. Without proceeding in the discouraging list of events which contribute to the description of the real world, we start our investigation by reducing the problem to the study of the simplest model arising in Celestial Mechanics: the two–body problem. Consider, for example, the motion of an asteroid about the Sun, neglecting all additional effects like the gravitational influence of the other planets. The solution of this simplified problem dates back to J. Kepler, according to which the asteroid revolves around the Sun on an elliptic orbit and the motion can be described by elementary formulae. The two–body problem is the archetype of an *integrable* system, for which an explicit solution can be found.

According to our strategy we increase the difficulty of the problem, just adding the effect of a third body, for example Jupiter, the largest planet of the solar system. The three–body problem has been investigated since the XVIII century by several astronomers and mathematicians. However, an explicit solution cannot be found. Indeed, H. Poincaré ([48]) proved that the three–body problem is *non–integrable*, since there are not sufficiently many independent integrals (namely, quantities which are constant during the evolution of the dynamics), allowing to derive mathematical expressions which describe the motion of an asteroid under the Newtonian attraction of the Sun and Jupiter. Since the mass of Jupiter is much smaller than that of the Sun (the mass ratio amounts to about 10^{-3}), the asteroid–Sun–Jupiter problem is close to the asteroid–Sun integrable system whose solution is provided by Kepler's laws. Therefore the effect of Jupiter can be considered as a small perturbation and the three–body problem enters the class of the so–called *nearly–integrable* systems. In this case, even if the complete answer cannot be given, one can proceed trying to find an *approximate* solution of the equations of motion, which describe the dynamics with *sufficient* accuracy. The development of this kind of approach is known as *perturbation theory*, which we shall describe in the next section.

In order to make these concepts quantitative, let us consider a mechanical system with n

degrees of freedom, described by the Hamiltonian function $\tilde{H}(\underline{p},\underline{q})$, where $\underline{p} \in \mathbf{R}^n$, $\underline{q} \in \mathbf{R}^n$. If the system is integrable, there exists a canonical change of variables $\mathcal{C} : (\underline{I},\underline{\varphi}) \in \mathbf{R}^n \times \mathbf{T}^n \to (\underline{p},\underline{q}) \in \mathbf{R}^{2n}$ (with $\mathbf{T} \equiv \mathbf{R}/2\pi\mathbf{Z}$), such that the transformed Hamiltonian becomes

$$H \circ \mathcal{C}(\underline{I},\underline{\varphi}) = h(\underline{I}) ,$$

having the property to depend only on the variables $\underline{I}$. The coordinates $(\underline{I},\underline{\varphi})$ are known in the literature as *action–angle* variables ([4]). The integrability of the system can be immediately recognized by writing down Hamilton's equations. In fact, denoting by

$$\underline{\omega} = \underline{\omega}(\underline{I}) = \frac{\partial h(\underline{I})}{\partial \underline{I}}$$

the *frequency* or *rotation number* of the system, one has

$$\begin{aligned} \dot{\underline{I}} &= \frac{\partial h(\underline{I})}{\partial \underline{\varphi}} = \underline{0} \\ \dot{\underline{\varphi}} &= \frac{\partial h(\underline{I})}{\partial \underline{I}} = \underline{\omega}(\underline{I}) . \end{aligned}$$

Therefore, the vector $\underline{I}$ is constant during the motion, say $\underline{I} = \underline{I}_0$, while from the second equation we have $\underline{\varphi} = \underline{\omega}(\underline{I}_0)t + \underline{\varphi}_0$, where $(\underline{I}_0, \underline{\varphi}_0)$ denote the initial conditions.

A nearly–integrable system can be conveniently described in terms of a Hamiltonian of the form

$$H(\underline{I},\underline{\varphi}) \;=\; h(\underline{I}) + \varepsilon f(\underline{I},\underline{\varphi}) , \tag{1}$$

where $h(\underline{I})$ represents the integrable part, while $\varepsilon f(\underline{I},\underline{\varphi})$ is the perturbation whose size, measured by the parameter ε, is supposed to be small.

The dynamics associated to the three–body problem can be described in terms of a nearly–integrable Hamiltonian system of the previous form. Indeed, referring to the example of the motion of the asteroid under the attraction of the Sun and Jupiter, the integrable part represents the two–body asteroid–Sun interaction (whose solution is given by Kepler's laws), while the perturbation is due to the gravitational influence of Jupiter; in particular, the perturbing parameter ε represents the Jupiter-Sun mass ratio. Though an explicit solution of this problem cannot be found, perturbation theory can provide useful tools to predict the motion within good accuracy.

2.2 Perturbation theory

Celestial Mechanics stimulated the development of perturbation theory. To give an example, thanks to unexplained perturbations on the motion of Uranus, the discovery of the planet Neptune was anticipated theoretically by J. Adams and U. Leverrier; their mathematical computations, performed using perturbation theory, predicted the position of Neptune with astonishing accuracy.

In order to explore in more detail the fundamentals of perturbation theory ([4], [5], [25], [50]), let us start by considering a Hamiltonian function of the form (1). Neglecting the perturbation, we can solve explicitly the equations corresponding to the Hamiltonian $h(\underline{I})$; this provides an ε–approximation of the true solution up to a time of the order of $1/\varepsilon$. The goal of perturbation theory is to introduce a suitable change of coordinates such that we can integrate the equations of motion for a longer time. In particular, we describe a simple algorithm which allows to remove the perturbation to order ε^2. More precisely, we define a convenient change of variables, say $\mathcal{C} : (\underline{I}', \underline{\varphi}') \to (\underline{I}, \underline{\varphi})$ with the property that the transformed Hamiltonian $H'(\underline{I}', \underline{\varphi}')$ takes the form

$$H'(\underline{I}', \underline{\varphi}') \;=\; H \circ \mathcal{C}(\underline{I}', \underline{\varphi}') \;\equiv\; h'(\underline{I}') + \varepsilon^2 f'(\underline{I}', \underline{\varphi}') \ , \qquad (2)$$

with suitable functions h' and f'. We remark that the perturbing function has now been removed to orders ε^2 and therefore Hamilton's equations associated to (2) can be integrated up to a time of order $1/\varepsilon^2$. Since ε is a small quantity ($0 < \varepsilon << 1$) we get the solution of the motion for a longer time. This idea was developed since the XVIII century to compute the dynamics of the bodies of the solar system with more precision than Kepler's laws. The ingredients needed to implement perturbation theory are very elementary and are based on the construction of a coordinate's transformation, a Taylor series development as a function of the perturbing parameter ε and a Fourier series expansion to determine explicitly the change of coordinates.

It is rather instructive to derive a first order perturbation theory. We ask the reader to make a little effort in trying to follow the mathematical formulae, so that she/he can control the basics of the computations, which allow to make refined predictions of the solar system dynamics. Let us start by introducing the canonical change of variables $(\underline{I}, \underline{\varphi}) \to (\underline{I}', \underline{\varphi}')$ by means of the system of equations

$$\begin{aligned} \underline{I} &= \underline{I}' + \varepsilon \frac{\partial \Phi(\underline{I}', \underline{\varphi})}{\partial \underline{\varphi}} \\ \underline{\varphi}' &= \underline{\varphi} + \varepsilon \frac{\partial \Phi(\underline{I}', \underline{\varphi})}{\partial \underline{I}'} \ , \end{aligned}$$

where the *unknown* function $\Phi(\underline{I}', \underline{\varphi})$ is usually denoted as the *generating function*. We remark that Φ depends on the old angle variables $\underline{\varphi}$ and on the new action variables $\underline{I}'$, as usually defined in textbooks of classical mechanics (see, e.g., [4]). In order to give explicit formulae for the transformed Hamiltonian, let us start by splitting the perturbing function $f(\underline{I}, \underline{\varphi})$ into a part $f_0(\underline{I}) = \frac{1}{(2\pi)^n} \int_{\mathbf{T}^n} f(\underline{I}, \underline{\varphi}) d\underline{\varphi}$, depending only on the variables $\underline{I}$ and a remainder function $\tilde{f}(\underline{I}, \underline{\varphi})$

defined by the expression $\tilde{f}(\underline{I},\underline{\varphi}) \equiv f(\underline{I},\underline{\varphi}) - f_0(\underline{I})$. Next, we insert the change of variables in the Hamiltonian (1) and we expand in Taylor series up to the second order around $\varepsilon = 0$; more precisely, we obtain

$$\begin{aligned}
& h(\underline{I}' + \varepsilon \frac{\partial \Phi(\underline{I}',\underline{\varphi})}{\partial \underline{\varphi}}) + \varepsilon f(\underline{I}' + \varepsilon \frac{\partial \Phi(\underline{I}',\underline{\varphi})}{\partial \underline{\varphi}}, \varphi) \\
= \ & h(\underline{I}') + \underline{\omega}(\underline{I}') \cdot \varepsilon \frac{\partial \Phi(\underline{I}',\underline{\varphi})}{\partial \underline{\varphi}} + \varepsilon f_0(\underline{I}') + \varepsilon \tilde{f}(\underline{I}',\underline{\varphi}) + O(\varepsilon^2) \ ,
\end{aligned}$$

where we recall that $\underline{\omega} \equiv \frac{\partial h}{\partial \underline{I}}$. Since we want that the new Hamiltonian is integrable up the second power of ε, we need to kill the first order term in ε by requiring that the function Φ satisfies the equation

$$\underline{\omega}(\underline{I}') \cdot \frac{\partial \Phi(\underline{I}',\underline{\varphi})}{\partial \underline{\varphi}} + \tilde{f}(\underline{I}',\underline{\varphi}) = \underline{0} \ . \tag{3}$$

The above equation is well–posed, since its average over the angle variables is zero. If we succeed to find a solution of (3), then we immediately recognize that the new integrable Hamiltonian can be written as

$$h'(\underline{I}') \ = \ h(\underline{I}') + \varepsilon f_0(\underline{I}') \ ,$$

whose associated Hamilton's equations provide the solution of the motion up to $O(\varepsilon^2)$. The equation (3) can be used to derive an explicit expression for the generating function. More precisely, let us expand the functions Φ and $\tilde{f}$ in Fourier series as

$$\begin{aligned}
\Phi(\underline{I}',\underline{\varphi}) \ &= \sum_{\underline{m}\in\mathbf{Z}^n\backslash\{\underline{0}\}} \hat{\Phi}_{\underline{m}}(\underline{I}') \ e^{i\underline{m}\cdot\underline{\varphi}} \ , \\
\tilde{f}(\underline{I}',\underline{\varphi}) \ &= \sum_{\underline{m}\in\mathbf{Z}^n\backslash\{\underline{0}\}} \hat{f}_{\underline{m}}(\underline{I}') \ e^{i\underline{m}\cdot\underline{\varphi}} \ .
\end{aligned}$$

Inserting the Fourier expansion inside (3) we obtain

$$i \sum_{\underline{m}\in\mathbf{Z}^n\backslash\{\underline{0}\}} \underline{\omega}(\underline{I}') \cdot \underline{m} \ \hat{\Phi}_{\underline{m}}(\underline{I}') \ e^{i\underline{m}\cdot\underline{\varphi}} = - \sum_{\underline{m}\in\mathbf{Z}^n\backslash\{\underline{0}\}} \hat{f}_{\underline{m}}(\underline{I}') \ e^{i\underline{m}\cdot\underline{\varphi}} \ ,$$

from which we derive

$$\hat{\Phi}_{\underline{m}}(\underline{I}') = - \frac{\hat{f}_{\underline{m}}(\underline{I}')}{i \ \underline{\omega}(\underline{I}') \cdot \underline{m}} \ .$$

Casting together the above formulae, we obtain that the generating function is given by the expression

$$\Phi(\underline{I}',\underline{\varphi}) = i \sum_{\underline{m}\in\mathbf{Z}^n\backslash\{\underline{0}\}} \frac{\hat{f}_{\underline{m}}(\underline{I}')}{\underline{\omega}(\underline{I}') \cdot \underline{m}} \ e^{i\underline{m}\cdot\underline{\varphi}} \ .$$

We strongly remark that the algorithm presented above is constructive in the sense that it allows to give explicit formulae for the computation of the transformed Hamiltonian as well as of the canonical change of variables. However, there could be a problem in the above implementation whenever the terms $\underline{\omega}(\underline{I}')\cdot\underline{m}$ are zero, meaning that the frequency vector is rationally dependent. In such case, the generating function is not defined and the algorithm fails. Indeed, if the vector $\underline{\omega}$ is rationally independent, the divisors are not identically zero, but they can become arbitrarily small and they can lead to the divergence of the series defining the generating function. The *small divisor* problem is the obstacle which prevents the iteration of the algorithm described above to higher orders in ε. If the divisors are very small, the Fourier coefficients defining the generating function become very big and it may happen that the series does not converge. However, the theory founded by A.N. Kolmogorov in 1954 allows to iterate infinitely many times the above procedure and, under suitable assumptions, to prove the existence of *stable* motions.

2.3 The Kolmogorov–Arnold–Moser theorem

The success of perturbation theory crucially depends on the character of the frequency vector $\underline{\omega}$. Let us focus on the case of $\underline{\omega} = (\omega_1, ..., \omega_n)$ being rationally independent, namely there do not exist a vanishing linear combination with rational coefficients (unless all the coefficients are zero). A *quasi–periodic* motion is a solution that can be expressed (as the time t varies) as a function of the form $F = F(\omega_1 t, ..., \omega_n t)$, where $F(\varphi_1, ..., \varphi_n)$ is a multiperiodic function, 2π–periodic in the angles φ_i and $\underline{\omega}$ is rationally independent. In order to illustrate the difference between periodic and quasi–periodic motions, let us consider the dynamics on a two–dimensional torus (i.e., fix $n = 2$), which is graphically represented by a life–belt. A point on the torus is located introducing two angles φ_1, φ_2 (with $0 \leq \varphi_1 \leq 2\pi$, $0 \leq \varphi_2 \leq 2\pi$) measured on the parallel and on the meridian of the torus. If we assume that the evolution is given by $\varphi_1(t) = \omega_1 t + \varphi_1(0)$, $\varphi_2(t) = \omega_2 t + \varphi_2(0)$, the difference between periodic and quasi–periodic motions is related to the rational or irrational character of the quantity $\frac{\omega_1}{\omega_2}$. In particular, if $\frac{\omega_1}{\omega_2}$ is a rational number, say $\frac{\omega_1}{\omega_2} = \frac{p}{q}$ with $p, q \in \mathbf{Z}_+$, then the motion is periodic and it retraces the same steps. On the contrary, if $\frac{\omega_1}{\omega_2}$ is irrational, the evolution never returns to the initial position and it can be shown that the trajectory is everywhere dense on the torus, defining a quasi–periodic motion ([2]).

As described in section 2.2, perturbation theory concerns the fate of the solutions of an integrable system under a small perturbation which preserves the Hamiltonian structure. Standard theories approached this problem by fixing the initial conditions and by investigating the consequent evolution. Instead of looking for the stability of the solution with preassigned initial conditions, Kolmogorov changed point of view by investigating the stability of the dynamics with a fixed frequency $\underline{\omega}$. At the International Congress of Mathematicians held in Amsterdam in 1954, Kolmogorov announced a result which marked a milestone in the development of the stability theory of nearly–integrable Hamiltonian systems ([32]).

Kolmogorov's theorem can be stated as follows: consider a real–analytic Hamiltonian function of the form (1) and fix a rationally independent frequency vector $\underline{\omega}$; under suitable assumptions on the unperturbed Hamiltonian h and on the frequency $\underline{\omega}$, if the strength of the perturbation (namely the parameter ε) is sufficiently small, there exists an invariant torus on which a quasi–periodic motion with frequency $\underline{\omega}$ takes place. Moreover, Kolmogorov's theorem states that the collection of such invariant tori form a set of positive measure in the phase space. In [32] Kolmogorov gave also an outline of the proof: such scheme turned out to be particularly rich and useful. In 1963 V.I. Arnold ([1], [2]) published a detailed alternative proof of Kolmogorov's theorem, while in 1962 J. Moser ([44]) developed a proof about the existence of invariant curves for smooth enough area–preserving mappings in the plane. Since then, the overall theory is known with the acronym of KAM theory.

In order to illustrate KAM theory in more detail, let us consider a Hamiltonian function of the form (1). As far as the integrable system is concerned (namely setting $\varepsilon = 0$), we have seen that Hamilton's equations lead to quasi–periodic motions where the actions are constant, say $\underline{I} = \underline{I}_0$ with $\underline{\omega}(\underline{I}_0) \equiv \underline{\omega}_0$, while the angles vary linearly with the time ($\underline{\varphi}(t) = \underline{\omega}_0 t + \underline{\varphi}_0$). The assumptions under which KAM theory can be applied are very general. The first hypothesis concerns the unperturbed Hamiltonian $h(\underline{I})$ which we assume to be *non–degenerate*, in the sense that the determinant of the Hessian matrix is different from zero [1]:

$$\det \frac{\partial^2 h(\underline{I})}{\partial \underline{I}^2} \neq 0 \ , \qquad \forall \ \underline{I} \in \mathbf{R}^n \ . \tag{4}$$

The second assumption concerns the frequency vector: in order to avoid the small–divisor problem, one requires that $\underline{\omega}_0$ satisfies a strong irrationality condition, namely that $\underline{\omega}_0$ fulfills the *diophantine* inequalities:

$$|\underline{\omega}_0 \cdot \underline{m}|^{-1} \ \leq \ C|\underline{m}|^\tau \ , \qquad \forall \ \underline{m} \in \mathbf{Z}^n \backslash \{\underline{0}\} \ , \tag{5}$$

where C, τ are positive constants. We remark that the above assumption is more stringent than requiring a *non–resonance* condition of the form $|\underline{\omega}_0 \cdot \underline{m}| \neq 0$ for any $\underline{m} \in \mathbf{Z}^n \backslash \{\underline{0}\}$.

Since the diophantine condition (5) plays a key role in the statement of the KAM theorem, we want to make it clearer through a concrete example. Take $n = 2$ and assume that the frequency vector has the form $\underline{\omega}_0 \equiv (\gamma, 1)$ with γ being a real number. Let us introduce the *continued fraction* representation of the number γ as the sequence of positive integers $\{a_0, a_1, a_2, a_3 ...\}$, such that

$$\gamma = a_0 + \frac{1}{a_1 + \frac{1}{a_2 + \frac{1}{a_3 + \dots}}} \ .$$

[1]Notice that the non–degeneracy condition implies that the frequencies satisfy the relation: $\det \frac{\partial \underline{\omega}(\underline{I})}{\partial \underline{I}} \neq 0$.

Using a standard notation, we write $\gamma = [a_0; a_1, a_2, ...]$. A simple computation shows that if γ is a rational number, then its continued fraction is composed by a finite number of terms: there exists a positive integer N such that $\gamma = [a_0; a_1, a_2, ..., a_N]$. On the contrary, if γ is an irrational number, then the continued fraction representation is infinite. Number theory guarantees that the diophantine condition (5) with $\tau = 1$ is satisfied, for example, by the so–called *noble* numbers, i.e. irrational numbers whose continued fraction is definitely 1: there exists a positive integer M such that $\gamma = [a_0; a_1, a_2, ..., a_M, 1, 1, 1, ...]$. Obviously, the most "noble" irrational number is represented by a continued fraction composed by all 1's; this number, known since antiquity, is the *golden ratio* $\frac{\sqrt{5}+1}{2} = [1; 1, 1, 1, ...]$. The golden ratio satisfies condition (5) with the smallest diophantine constant C, being $C = \frac{3+\sqrt{5}}{2}$. Finally, let us mention that each irrational number can be approximated by a sequence of rational numbers $\{\frac{p_k}{q_k}\}_{k\in\mathbf{Z}}$ provided by the successive truncations of the continued fraction, i.e.

$$\frac{p_1}{q_1} = a_0 + \frac{1}{a_1}\ , \qquad \frac{p_2}{q_2} = a_0 + \frac{1}{a_1 + \frac{1}{a_2}}\ , \qquad \frac{p_3}{q_3} = a_0 + \frac{1}{a_1 + \frac{1}{a_2 + \frac{1}{a_3}}} \ ...$$

For the golden ratio, the rational approximants are given by the ratio of the so-called Fibonacci's numbers and the sequence $\{1, \frac{2}{1}, \frac{3}{2}, \frac{5}{3}, \frac{8}{5}, \frac{13}{8}, \frac{21}{13}, ...\}$ converges to $\frac{\sqrt{5}+1}{2}$.

Coming back to the description of the content of KAM theory, let us consider a Hamiltonian system described by (1), assuming that the conditions (4) and (5) are satisfied. We ask ourselves whether there still exists for the perturbed problem (namely taking $\varepsilon \neq 0$) an invariant torus on which a quasi–periodic motion with frequency $\underline{\omega}_0$ takes place. KAM theory yields a positive answer to this question, provided that the size of the perturbing parameter ε is sufficiently small, say $\varepsilon \leq \varepsilon_{KAM}(\underline{\omega}_0)$. The smallness condition is required in order to guarantee the convergence of the series developments involved in the proof. We remark that for low–dimensional iso–energetically non–degenerate Hamiltonian systems, the existence of a KAM torus provides a strong stability property. More precisely, if $n = 2$ the phase space has dimension 4 and the constant energy surfaces have dimension 3. Therefore, the 2–dimensional KAM tori foliate the constant energy levels providing the stability of the motion, due to the uniqueness of the solutions of ordinary differential equations. This property ceases to be valid as $n \geq 3$; indeed, already if $n = 3$ the dimensions of the phase space and of the constant energy surfaces are, respectively, 6 and 5. Thus, the 3–dimensional KAM tori do not provide a separation of the phase space into invariant regions as it is the case for the 2–dimensional Hamiltonian systems.

Before having an insight on the proof of the KAM theorem, let us briefly describe the qualitative behaviour of the KAM torus as the perturbing parameter is varied. If ε is very small, the invariant torus lives close to the location of the unperturbed torus, but it becomes more and more displaced and deformed as the perturbing parameter increases. At a certain value of ε, say $\varepsilon = \varepsilon_c(\underline{\omega}_0)$, the invariant torus ceases to be regular and for $\varepsilon > \varepsilon_c(\underline{\omega}_0)$ breaks down. In order to estimate the critical break–down threshold of an invariant torus with frequency $\underline{\omega}_0$, we can use the analytical approach given by the KAM theorem to get a lower bound $\varepsilon_{KAM}(\underline{\omega}_0)$. Alternatively, we can implement a numerical investigation to determine the break–down value $\varepsilon_c(\underline{\omega}_0)$. Along this direction, the most used numerical method is due to J. Greene ([26]), who provided an efficient algorithm to compute the critical threshold. The original work ([26]) has been developed for a simple discrete system known as the *standard mapping*, characterized by a single frequency $\omega_0 \in \mathbf{R}$. Greene's method relies on the conjecture that the break–down of an invariant surface with frequency ω_0 is strictly related to the transition from stability to instability of the periodic orbits with frequency given by the rational approximants $\{\frac{p_k}{q_k}\}_{k\in\mathbf{Z}}$ converging to ω_0. The stability character of the periodic orbits can be easily determined by computing the Lyapunov's exponents; therefore, Greene's method can be easily adapted to numerical computations and it has been extensively applied to a wide variety of continuous and discrete systems. Partial proofs of Greene's technique has been presented in [17], [42].

Concerning the analytical estimate, the idea behind Kolmogorov's theorem is to overcome the small divisor problem by producing a *superconvergent* sequence of canonical transformations. We reviewed in section 2.2 the standard perturbation theory which allows to transform the initial Hamiltonian, say $H_1 = h_1 + \varepsilon f_1$, to a Hamiltonian denoted as $H_2 = h_2 + \varepsilon^2 f_2$, where the perturbation is, roughly speaking, of order ε^2. One can try to iterate the algorithm to obtain the Hamiltonian $H_3 = h_3 + \varepsilon^3 f_3$ and, at the j-th step, $H_j = h_j + \varepsilon^j f_j$. However, the hindrance due to the convergence of the method cannot be in general surmounted. The idea of Kolmogorov consists in the development of a *quadratic* method according to which the initial Hamiltonian is transformed to $H_2 = h_2 + \varepsilon^2 f_2$. Iterating one has $H_3 = h_3 + \varepsilon^4 f_3$ and, at the j-th step, $H_j = h_j + \varepsilon^{2^{(j-1)}} f_j$. The fact that the perturbation decreases with ε faster than linearly allows to control the small divisors appearing in the sequence of transformations.

Newton's method for finding the real root of an equation $f(\xi) = 0$ offers the opportunity to explain conveniently the difference between the linear (standard perturbation theory) and quadratic (KAM theory) methods (see Figure 1). Let us start with an initial approximation ξ_0 and let $e_0 \equiv |\xi - \xi_0|$ be an estimate on the initial error. If we proceed to find the solution by a *linear* convergence, the successive approximation ξ_1 is determined as the intersection of the tangent to the curve at the point $(\xi_0, f(\xi_0))$ with the ξ–axis. Let the derivative of f at ξ_0 be $\eta_0 \equiv f'(\xi_0)$. Next approximation ξ_2 is computed as the abscissa of the line through $(\xi_1, f(\xi_1))$ with slope η_0. Iterating this algorithm, the error at step j is $e_j = |\xi - \xi_j| = O(e_0^{j+1})$, in analogy to standard perturbation theory.

In the quadratic procedure, the successive approximations are computed as the intersection between the ξ–axis and the tangent to the function computed at the previous step, i.e.

$$\xi_{j+1} = \xi_j - \frac{f(\xi_j)}{f'(\xi_j)} \qquad j = 0, 1, 2...$$

Let us expand $f(\xi)$ around ξ_j; the second order expansion is given by

$$0 = f(\xi) = f(\xi_j) + f'(\xi_j)(\xi - \xi_j) + \frac{f''(\xi_j)}{2!}(\xi - \xi_j)^2 + O(|\xi - \xi_j|^3) ,$$

which yields

$$\xi_{j+1} - \xi = \frac{1}{2!} \frac{f''(\xi_j)}{f'(\xi_j)}(\xi - \xi_j)^2 .$$

Therefore, the error at the step j goes quadratically as

$$e_{j+1} = O(e_j^2) = O(e_0^{2^j}) .$$

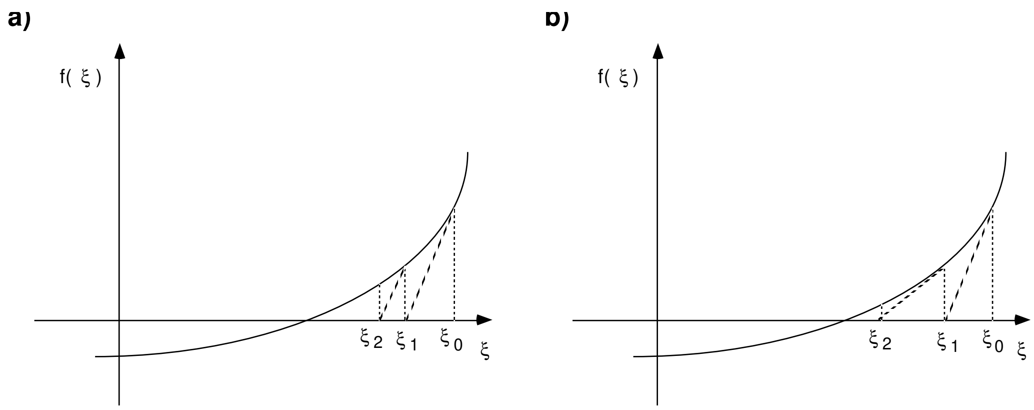

Figure 1: Newton's method for finding the root of the equation $f(\xi) = 0$. $a)$ Linear convergence; $b)$ quadratic convergence.

The proof of the KAM theorem requires a long set of estimates in order to ensure the convergence of the method. We refer the reader to [32], [1], [44], [5], [25], [50] for the detailed proof.

2.4 The stability of a model associated to the three–body problem

The study of the stability of the three–body problem in Celestial Mechanics has a long tradition. A mathematical approach based on first–order perturbation theory was introduced by Lagrange and Laplace. In particular, we focus on the effect of small perturbations on the dynamics of the planets in order to see whether, after sufficiently long time, collisions or escape to infinity might take place. In [2], the planetary motion in the framework of the three–body and many–body problems was investigated. Quoting directly V.I. Arnold ([2], p.125, see also [1]), his result is the following: *"for the majority of the initial conditions under which the instantaneous* *orbits of the planets are close to circles lying in a single plane, perturbation of the planets on one another produces, in the course of an infinite interval of time, little change on these orbits provided the masses of the planets are sufficiently small".* To give concrete estimates, M. Hénon ([29]) applied the original version of Arnold's theorem to the three–body problem, allowing to prove the existence of invariant tori for values of the perturbing parameter (namely the Jupiter–Sun mass ratio) less or equal than 10^{-333}. Such estimate was improved to 10^{-50} by applying Moser's theorem. However, astronomical observations show that the mass of Jupiter compared to that of the Sun is about 10^{-3}. The discrepancy between the KAM estimate and the physical value led to the idea that KAM theory is unable to produce effective results. Indeed, at least for some model problems, the refinement of the KAM estimates and *computer–assisted* series expansions provide results which are in agreement with the astronomical observations and numerical experiments ([8], [9], [10], [11], [12]). Let us describe a recent results obtained in [12] concerning the stability of some asteroids in a 3–body framework (see also [11]). We remind that asteroids are thousands minor bodies of the solar system which populate a belt between the orbits of Mars and Jupiter.

Let us introduce a mathematical model, which describes the motion of an asteroid moving under the gravitational influence of the Sun and Jupiter. We assume that the three bodies move on the same plane and that the mass of the asteroid is so small that it does not influence the motion of the primaries. Moreover, we assume that Jupiter orbits the Sun on a circular (Keplerian) orbit. This model is known as the *planar, circular, restricted three–body problem.* It can be conveniently described in terms of suitable action–angle coordinates, known as *Delaunay's variables* ([15], [51]) and the corresponding Hamiltonian function has two degrees of freedom. The unperturbed frequencies (namely the frequencies obtained considering the two–body problems provided by the pairs Sun–asteroid or Sun–Jupiter) are inversely proportional to the periods of revolution about the Sun. We remark that a resonance condition occurs whenever the ratio of the periods of revolution of the asteroid and of Jupiter about the Sun is a rational number; there are many examples in the asteroidal belt which meet such condition, usually denoted as *orbit–orbit resonance.*

With reference to section 2.3, since the Hamiltonian system is two–dimensional, we fix a level of energy (corresponding to the Keplerian motion of the asteroid) in order to have a control on the dynamics. The stability of the minor body can be obtained by proving the existence of invariant surfaces which confine the motion of the asteroid on the given energy level. Refined KAM estimates for the isoenergetic case have been developed in [12]. The proof involves heavy computations of the series expansion of the solution. To this end, a suitable implementation on the computer has been performed. We remark that the computer is used so that all numerical errors introduced by the machine are controlled through the so–called *interval arithmetic* technique, which is becoming a widespread tool to prove analytical results with the aid of the computer (we refer the reader to [33], [16], [31] and references therein for details about computer–assisted proofs). We want to stress that computer–assisted techniques are a complementary part in the proof of mathematical results.

The dynamics of the asteroids Iris, Victoria and Renzia have been considered; the application of the (isoenergetic, computer–assisted) KAM theory provides their stability for values of the perturbing parameter less or equal than 10^{-3}, giving a result in full agreement with the astronomical prediction. As a conclusion, we stress that this result contributes to show that beside solving the stability problem from a purely mathematical point of view, KAM theory turns out to be effective also in physical models.

3 Unstable motions

Quasi periodic motions have been investigated in the previous section, where we showed that the essential features are close to the integrable approximation. Within KAM theory, nothing is predicted for the initial conditions which do not satisfy the diophantine inequality (5). In order to have a complete representation of the phase space, we intend to explore the portion in which a resonance condition of the form $\sum_{i=1}^{n} k_i\omega_i = 0$ (with some integers $k_1, \ldots, k_n \in \mathbf{Z}\backslash\{0\}$) is satisfied in the integrable approximation. We define the *Arnold's web* as a suitable neighborhood of resonant orbits, whose size depends on the perturbing parameter and on the order of the resonance, i.e. $\sum_{i=1}^{n} |k_i|$. The trajectories in the Arnold's web can exhibit chaotic features.

The structure of the Arnold's web was clearly explained already in [3]; the numerical investigation of its structure has been recently performed on mathematical models ([35]) and on physically interesting systems. We remark that the stability analysis in the frame of KAM theory has touched different fields of physics. To give some examples, we mention the studies on beam-beam interactions ([43]), asteroids diffusion ([46]) and galactic models ([47]). These works have been based on numerical applications using frequency-map analysis ([37]). It is worthwhile to stress that the validity of the numerical investigations is not only explanatory or didactic; indeed, while KAM theorem describes the persistence of regular orbits, a rigorous proof of the existence of instability or irregularity in the Arnold web is a delicate problem.

In the following sections, we shall review a theoretical result due to Nekhoroshev and we will introduce a numerical tool ([24]), which allows to detect and to draw the Arnold's web in a very detailed way ([20]). Such analysis allows also to study the transition from a stable to a diffusive regime ([27]). We conclude by describing a numerical study ([39]) of the so–called Arnold's diffusion ([3]).

3.1 Nekhoroshev's theorem

A breakthrough in the solution of the problem of stability of a Hamiltonian quasi-integrable system is provided by Nekhoroshev's ([45]) theorem. Contrary to KAM theorem, Nekhoroshev result extends to an open set of initial conditions; the price to pay is that the stability for infinite times is replaced by the stability over *long* times. In particular, the stability time is exponentially long with respect to the inverse of the perturbing parameter. Therefore, the concept of long time stability is often equivalent in physical problems to that of effective stability. To give an example, the infinite time stability of Jupiter has no physical meaning since the solar system will end in some 5 billion years!

Nekhoroshev's theorem applies to quasi–integrable Hamiltonians of the form

$$H(\underline{I},\underline{\varphi}) = h(\underline{I}) + \varepsilon f(\underline{I},\underline{\varphi}) \ , \qquad (\underline{I},\underline{\varphi}) \in B \times \mathbf{T}^n \ , \tag{6}$$

where B is an open subset of $\mathbf{R}^n$ and $\mathbf{T}^n$ is the n–dimensional torus. We assume that h and f are analytic functions and that ε is a small parameter. Moreover, the integrable approximation h is required to satisfy a suitable geometric condition, called *steepness* ([45], see also [28],[6]). In the following, we will assume for simplicity that h is a convex function (convex functions satisfy the steepness condition). Under the above hypotheses, the theorem states that, if ε is sufficiently small, any solution $(\underline{I}(t),\underline{\varphi}(t))$ of (6) satisfies the following exponential estimate ([45], see also [7], [41], [49]):

$$\|\underline{I}(t) - \underline{I}(0)\| \leq I_0\, \varepsilon^a \qquad \text{for} \quad |t| \leq t_0\, e^{(\varepsilon_0/\varepsilon)^b} \ , \tag{7}$$

where $I_0, t_0, \varepsilon_0, a, b$ are suitable positive constants. In the convex case, one can take $a = b = 1/(2n)$ ([41], [49]). Therefore, for $\varepsilon < \varepsilon_0$, the actions remain close to their initial values up to exponentially long times. Unfortunately, as often occurs in perturbation theory, the purely analytical estimates of the constants I_0, t_0, ε_0 are quite unrealistic. This remark motivates the numerical studies for realistic models of physical interest.

The direct numerical check of the instability of the actions in general fails, since actions are bounded up to an exponentially long time. Therefore, alternative numerical tools have been developed in the last ten years to investigate the problem in an indirect way ([34], [37], [38], [14], [22]).

Actually, the hearth of the Nekhoroshev's theorem is that the long time stability of the actions occurs within a specific structure of the phase space: the core is made by a large part of KAM tori while the complementary part is structured by the Arnold's web. The numerical experiments are based on checking such peculiar structure of the phase space.

3.2 Tools for detecting chaos and order

In order to explore the phase space, a careful analysis of a large number of orbits is required. The classical tool for discriminating between chaotic and ordered orbits is the computation of the largest Lyapunov exponent, that we recall as follows. Let us consider the differential equations:

$$\tfrac{d}{dt}\underline{X} \quad = \quad \underline{F}(\underline{X}), \qquad \underline{X} = (x_1, x_2, ..., x_n) \tag{8}$$

where $\underline{F}$ are suitable regular functions. The Lyapunov exponents are computed by integrating the equations of motion (8), together with the corresponding variational equations:

$$\frac{d\underline{v}}{dt} = (\frac{\partial \underline{F}}{\partial \underline{X}})\, \underline{v} \ ,$$

where $\underline{v}$ is any n-dimensional vector. The largest Lyapunov exponent is defined as

$$\gamma = \lim_{t\to\infty} \ln \frac{||\underline{v}(t)||}{t} ;$$

let us remark that this limit does not always exist for $v(0)$ belonging to some subspaces of $\mathbf{R}^n$ ([19]). If (8) is of Hamiltonian type, the largest Lyapunov exponent is zero for regular motions and it is positive for chaotic orbits; this property has been largely used to discriminate between chaotic and ordered motions. However, among regular motions, the Lyapunov exponent does not allow to distinguish between KAM tori and resonant islands. When computing the Lyapunov exponents, the attention is focused on the length of time necessary to get a reliable value of the limit; very little importance has been given to the beginning of the integration, since it was considered a transitory regime, depending mainly on the choice of the initial vector on the tangent manifold.

As already remarked in [24], chaotic, even *weakly* chaotic, and ordered motion can be discriminated by looking at the value of $\log ||\underline{v}(T)||$, where T is relatively small. The authors called the above quantity Fast Lyapunov Indicator (hereafter FLI). It turns out that the FLIs allow also to distinguish among regular resonant and non resonant motions (see [27] for an analytic explication using a Hamiltonian system).

The precise definition of the FLI can be stated as follows: given an initial condition $\underline{X}(0) \in \mathbf{R}^n$ and an initial vector $\underline{v}(0) \in \mathbf{R}^n$, the FLI is provided by the relation ([20], [27])

$$FLI(\underline{X}(0), \underline{v}(0), T) \equiv \sup_{0<t\leq T} \log ||\underline{v}(t)|| , \qquad T \geq 0 \ .$$

In recent years other numerical tools have been introduced: the frequency map analysis ([34], [37], [35]), the sup-map analysis ([36], [21]) and the twist angle ([14], [22]). The twist angle is particularly suited for two dimensional area-preserving maps. The frequency map and the sup-map analyses can be applied to a generic system, but they are more expensive in terms of computational time ([23]). We remark that the FLI is defined for each kind of orbit, while the frequency is not well defined for chaotic orbits; moreover the FLI provides quantitative information about the measure of chaos.

3.2.1 The standard map as a model problem

The definition of the FLI can be extended to discrete systems as follows. Given a mapping M: $\mathbf{R}^n \to \mathbf{R}^n$, an initial condition $\underline{z}(0) \in \mathbf{R}^n$, and an initial vector $\underline{v}(0) \in \mathbf{R}^n$ of unitary norm, the

FLI function is provided by:

$$FLI(\underline{z}(0), \underline{v}(0), T) = \sup_{0<n\leq T} \log ||\underline{v}(n)||\,, \qquad T \geq 0\,,$$

where $\underline{v}(n)$ is defined through the set of coupled equations:

$$\begin{cases} \underline{z}(n+1) &= M(\underline{z}(n)) \\ \underline{v}(n+1) &= \frac{\partial M}{\partial \underline{z}}(\underline{z}(n))\ \underline{v}(n)\,. \end{cases}$$

As a model problem, we consider the two dimensional standard map ([18], [40], [13]):

$$M : \begin{cases} x(n+1) &= x(n) + \varepsilon \sin(x(n) + y(n)) \quad (\text{mod. } 2\pi) \\ y(n+1) &= y(n) + x(n) \qquad\qquad\qquad\quad (\text{mod. } 2\pi)\,. \end{cases} \tag{9}$$

In Figure 2, we display some orbits of the standard map defined by (9) with $\varepsilon = 0.6$. For

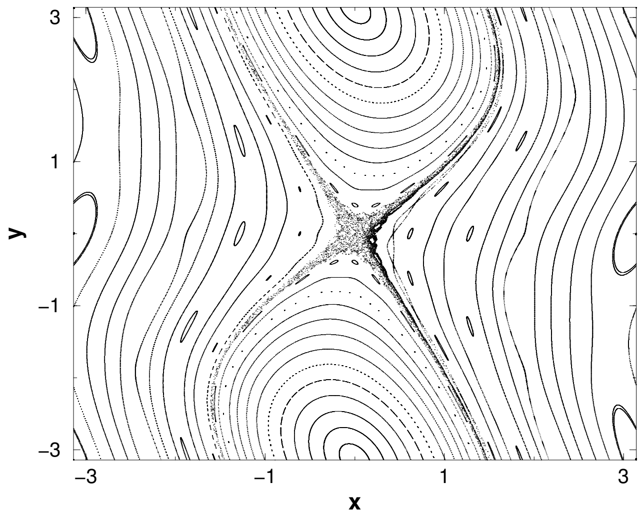

Figure 2: A set of orbits of the standard map for $\varepsilon = 0.6$.

$\varepsilon = 0.6$, the majority of the orbits are still invariant tori. Some resonant curves are displayed around elliptic points and a chaotic zone is generated by the existence of the hyperbolic point at the origin.

Figure 3 shows the variation of the FLI with respect to time for three different kinds of orbits. The upper curve, corresponding to initial conditions $(x, y) = (10^{-4}, 0)$ selected in the previous chaotic zone, shows an exponential increase of the FLI; the upper value of 20 is a threshold that we impose in order to avoid floating overflow. The intermediate curve corresponds to a regular invariant torus with initial conditions $(x, y) = (1, 0)$ and the lowest one describes a resonant trajectory with initial conditions $(x, y) = (0, 1)$.

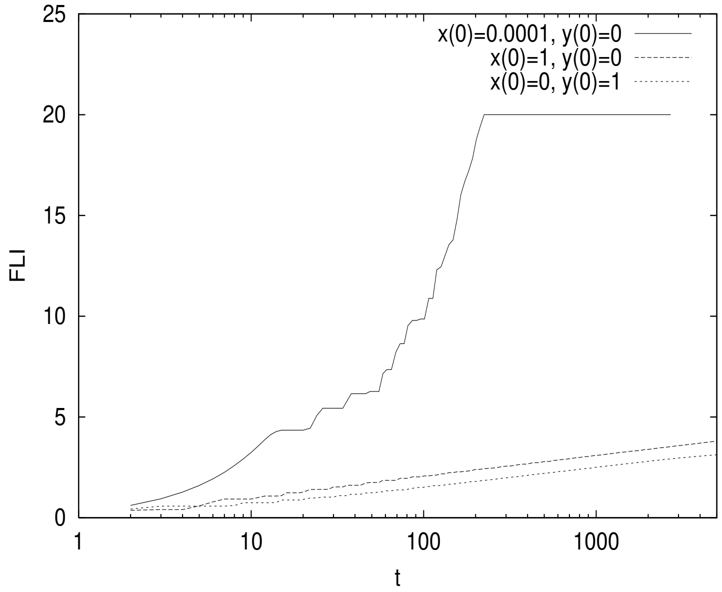

Figure 3: Variation of the Fast Lyapunov Indicator w.r.t. time for three orbits of the standard map with $\varepsilon = 0.6$. The upper curve corresponds to a chaotic orbit with initial conditions $x(0) = 10^{-4}, y(0) = 0$; the middle one describes a non–resonant orbit with $x(0) = 1, y(0) = 0$ and the lowest one concerns a resonant orbit with $x(0) = 0, y(0) = 1$.

In [23] the FLI was computed for a set of 1000 initial conditions, regularly spaced on the x-axis in the interval $[0, \pi]$, while $y(0)$ was always set to zero. Figure 4 shows the so called *FLI-map*, i.e. the value of the FLI after $T = 1000$ iterations against $x(0)$; here, $\underline{v}(0)$ was always taken in the direction of the x-axis. Many orbits appear to have an FLI equal to the logarithm of the integration time, i.e. $\log T = 3$: actually, this value corresponds to invariant tori ([23], [27]).

Values slightly greater than $\log T$ indicate very thin chaotic layers or invariant tori close to very thin chaotic zones. The orbits with an FLI lower than $\log T$ correspond to chains of islands (for an explanation see [27]).

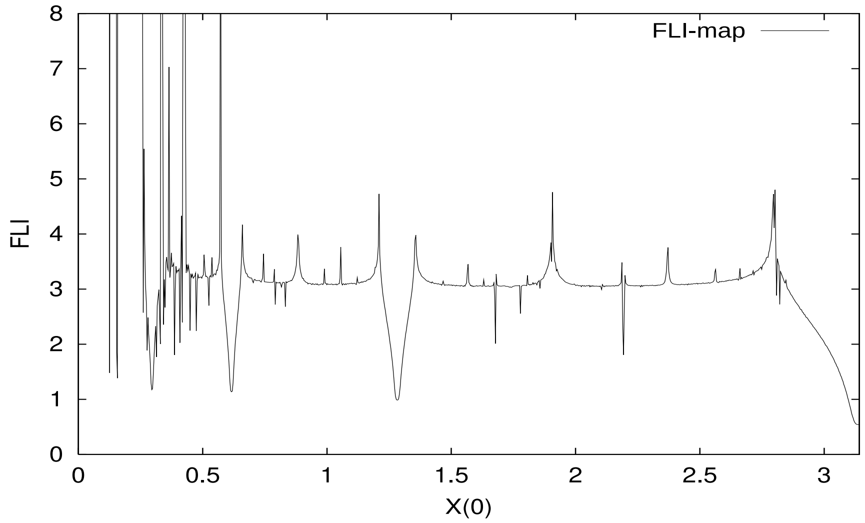

Figure 4: Variation of the FLI as a function of the initial values $x(0)$ for a set of 1000 orbits regularly spaced in the interval $[0, \pi]$. The initial vector $\underline{v}(0)$ has components $(1, 0)$, i.e. it is almost perpendicular to the corresponding invariant curves.

3.3 The Arnold's web pictures for a simple Hamiltonian model

In this section we give a high accurate graphical representation of the Arnold web, obtained implementing the FLI method. As an example, we consider the following Hamiltonian function:

$$H_\varepsilon(I_1, I_2, I_3, \varphi_1, \varphi_2, \varphi_3) = \frac{I_1^2}{2} + \frac{I_2^2}{2} + I_3 + \varepsilon \left(\frac{1}{\cos(\varphi_1) + \cos(\varphi_2) + \cos(\varphi_3) + 4} \right) \quad ,$$

where $I_1, I_2, I_3 \in \mathbf{R}$ and $\varphi_1, \varphi_2, \varphi_3 \in \mathbf{T}$ are canonically conjugated, and ε is a small parameter. The canonical equations of the integrable Hamiltonian H_0 are trivially integrated: I_1, I_2, I_3 stay constant, while the angles $\varphi_1(t) = \varphi_1(0) + I_1 t$, $\varphi_2(t) = \varphi_2(0) + I_2 t$, $\varphi_3(t) = \varphi_3(0) + t$ rotate with constant angular velocity. Therefore, each pair of actions (I_1, I_2) characterizes an invariant torus $\mathbf{T}^3$, on which motions are quasi–periodic with frequencies $\omega_1 = I_1$, $\omega_2 = I_2$, $\omega_3 = 1$. Conversely, for any whatsoever small ε different from zero, H_ε is not integrable. However, KAM theorem provides the existence of a large volume of invariant tori, embedded in the Arnold web. Our goal is to determine numerically the structure of the Arnold web, which can be conveniently represented in the two–dimensional plane (I_1, I_2). Indeed, each point on this plane corresponds to a unique frequency of an unperturbed torus. Moreover, all resonances $k_1\omega_1 + k_2\omega_2 + k_3\omega_3 = 0$ are represented by the straight lines $k_1 I_1 + k_2 I_2 + k_3 = 0$; the set of all resonances is dense on the plane. However, one can expect that irregular orbits surround each resonance line, up to a distance decreasing as $\sqrt{\varepsilon}/|k|^\tau$; we refer to this region as the *resonant zone*. Consequently, the volume of the Arnold web is of the order of $\sqrt{\varepsilon}$. We shortly review the qualitative behaviour of the motions with initial conditions in the Arnold web. Within resonant zones, both chaotic and regular motions can be observed. Stable periodic orbits are surrounded by islands on which the motion is still quasi-periodic, though the dimension of the torus is strictly smaller than the number of degrees of freedom. Unstable periodic orbits are surrounded by chaotic zones where Nekhoroshev's theorem predicts a diffusion with a velocity exponentially small with respect to $-1/\varepsilon$ in the action space. When increasing the strength of the perturbation, the regular set shrinks until it almost completely disappears. In this case the dynamics is no more controlled by Nekhoroshev's theorem. To describe it, we resort to the well known Chirikov ([13]) overlapping criterium, which allows the resonant chaotic orbits to go from one resonance to the other (eventually giving rise to large scale diffusion).

3.3.1 From Nekhoroshev to Chirikov

Using the FLI method, we proceed to describe the evolution from a mostly ordered system to a largely chaotic one, i.e. from the Nekhoroshev to the Chirikov regime. To this end, we computed the FLI, using a leap-frog symplectic integrator on a grid of 500×500 initial conditions regularly spaced in the action space (without loss of generality, we set the initial angles $\varphi_1 = \varphi_2 = \varphi_3 = 0$). The initial choice of the tangent vector plays a delicate role. Indeed, it turns out that resonances which are aligned with the initial tangent vector $(\dot{\varphi}_1, \dot{\varphi}_2)$ are not detected by the FLI method. In order to overcome this problem we have chosen $(\dot{\varphi}_1, \dot{\varphi}_2)$, such that $\dot{\varphi}_1/\dot{\varphi}_2$ is strongly irrational (the other components $\dot{I}_1, \dot{I}_2$ play a minor role and we set them equal to unity). Some results are presented in Figure 5. In each picture, the initial conditions of I_1 and I_2 are associated to the corresponding FLI value by a different colour. The lowest values of the FLI appear in black and they correspond to the resonant islands of the Arnold web; the highest values appear in yellow and they correspond to chaotic motions, arising at the crossing nodes of resonant lines or arising near the separatrices. The FLIs corresponding to KAM tori have approximately the same value and therefore they have the same colour (orange in Figure 5 (top, left), purple in the other figures). Therefore, the resonant lines clearly appear to embed large zones filled by KAM tori (see Figure 5 (top, left) and the enlargement shown in Figure 5 (top, right)). The choice of the colour varies with the value of the perturbing parameter and with the integration time. Since the perturbation has a full Fourier spectrum, i.e. all harmonics are present at order ε, a high number of resonances is already present for small ε (Figure 5 (top)); we remark that all resonances should appear just by increasing the integration time. On the contrary in Figure 5 (middle), which refers to $\varepsilon = 0.01$, the volume of the invariant tori decreases, though the system is still in the Nekhoroshev regime. In these figures, following Nekhoroshev theorem, the chaotic regions become evident at the crossing of the resonances. In Figure 5 (bottom), which refers to $\varepsilon = 0.04$, the dynamical regime has completely changed. As outlined before, the majority of invariant tori has disappeared due to resonance overlapping, and a big chaotic connected region replaced the regularity set.

In conclusion, using a very simple numerical tool, we described the structure of the Arnold web and its evolution as a function of the perturbing parameter. We observed a transition from an ordered to a chaotic diffusive system, occurring for $0.01 < \varepsilon_0 < 0.04$ (ε_0 being defined by (7)).

3.3.2 Detection of the diffusion

Following Nekhoroshev's theorem, we expect a very slow diffusion of the actions along the resonances, which is very difficult to detect numerically. The idea of such kind of diffusion was introduced by the pioneering work of Arnold ([3]), using an ad hoc model. Since then, it is called *Arnold's diffusion*. According to (7), when ε is close to ε_0, i.e. to the transition from the stable regime to the diffusive one, the actions can become quickly unstable. Therefore, in order to measure Arnold's diffusion, we need to start close to ε_0. In the previous section, we found that the transition occurred in the interval $0.01 < \varepsilon_0 < 0.04$ (this interval was confirmed and refined to $0.0300 < \varepsilon_0 < 0.032$ in [27]). We used the FLI pictures to find chaotic initial conditions on a given resonant line as well as to observe that diffusion occurs along this line.

Figure 6 shows some enlargements of the FLI pictures in the action space, around $I_1 = 0.3$, $I_2 = 0.14$ and for different values of ε. The region between the two yellow lines corresponds to the resonance associated to $I_1 - 2I_2 = 0$, while the two yellow lines correspond to its hyperbolic border where diffusion is confined. The graphical inspection provides the possibility of choosing initial data in the hyperbolic border. We can follow the evolution of the solution computing the double section of the solution: $\sigma = |\varphi_1| + |\varphi_2| \leq 0.05$, $\varphi_3 = 0$. This strategy allows to minimize all projection effects and fast quasi-periodic motions; henceforth, we can observe a very slow drift along the border of the resonance.

We considered 100 initial conditions in the interval $0.303 \leq I_1 \leq 0.304$, $0.143 \leq I_2 \leq 0.144$, having FLI values larger than $1.2 \cdot \log(T)$; such initial data generate chaotic orbits at the border of the resonance and they are chosen far from the more stable crossing with other resonances. Let us remark that the points in the double section will appear on both sides of the resonance (in fact the two yellow lines are connected by a hyperbolic region in the six dimensional phase space).

Figure 6 (top, left) provides the successive intersections with $\sigma \leq 0.05$, $\varphi_3 = 0$, up to a time $t = 10^7$; Figure 6 (top, right) extends to $t = 10^8$. Even if the perturbing parameter is one order of magnitude lower than the threshold ε_0, the diffusion phenomenon along the resonant line clearly appears. When decreasing ε to the minimum value $\varepsilon = 0.001$, we detected diffusion along the resonance with smaller and smaller speed. For $\varepsilon = 0.007$ (Figure 6 (middle, left) for $t = 10^6$, Figure 6 (middle, right) for $t = 2.4 \cdot 10^7$), one obtains similar results, though the speed of diffusion is larger. For $\varepsilon = 0.02$ (Figure 6 (bottom, left) for $t = 1.6 \cdot 10^4$, Figure 6 (bottom, right) for $t = 5 \cdot 10^5$), diffusion along the resonance is still evident, although it extends a little also on the direction transversal to the resonance. This phenomenon is due to the fact that

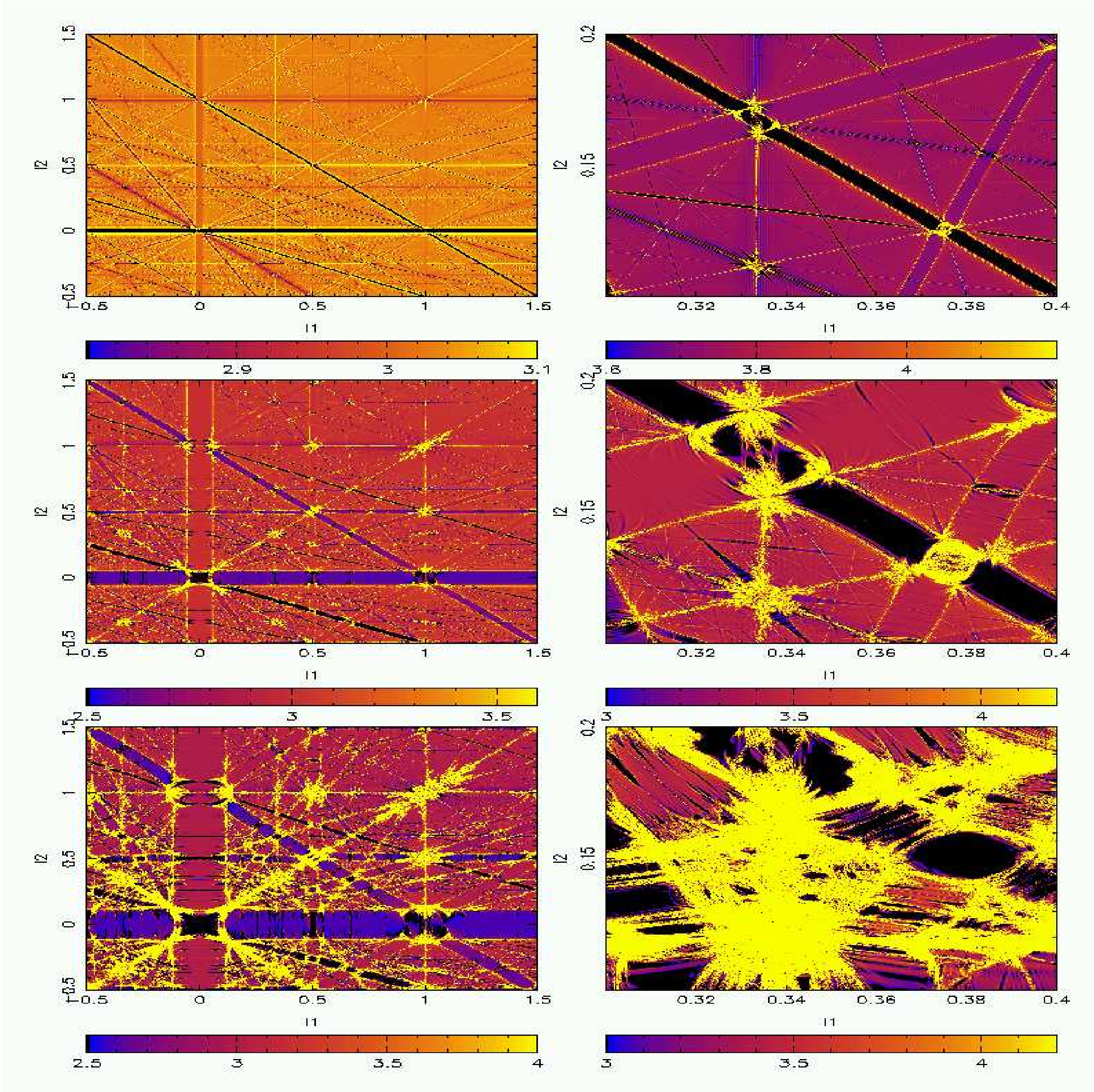

Figure 5: Evolution of the Arnold web for increasing values of the perturbing parameter ε. The lowest values of the FLI appear in black for the regular resonant islands; the highest values appear in yellow for chaotic motions arising at the crossing nodes of resonant lines or arising near the separatrix. The FLI corresponding to KAM tori have about the same value, represented in the picture by the same colour (orange: top left, purple the others). The colours are adapted to the choice of ε and of the integration time. Left column: a large portion of the action plane; top: $\varepsilon = 0.001$, $T = 1000$; middle: $\varepsilon = 0.01$, $T = 1000$; bottom: $\varepsilon = 0.04$, $T = 1000$. Right column: enlargement of the figures on the left, obtained with a larger integration time; top: $\varepsilon = 0.001$, $T = 4000$; middle: $\varepsilon = 0.01$, $T = 2000$; bottom: $\varepsilon = 0.04$, $T = 2000$ (from [20]).

we are approaching the transition value and higher order resonances intersecting the main one become evident. When approaching the critical value, we expect that a large chaotic region replaces the zone of invariant tori, giving rise to fast diffusion.

3.3.3 Measuring the diffusion coefficient

Though it does not exist yet an exhaustive analytic model, we tried to measure a diffusion coefficient as if the phenomenon was Brownian like. The numerical experiments are constrained by computational limitations, since we have to find a compromise between the number of initial conditions and the length of the integration time. Anyway, we could confirm the Brownian hypothesis, i.e. we observed an averaged linear increase with time, with slope D, of the mean squared distance from the initial conditions. More precisely we computed the quantity:

$$S(t) = \frac{1}{N}\sum_{j=1}^{N}[(I_{2,j}(t) + 2I_{1,j}(t)) - (I_{2,j}(0) + 2I_{1,j}(0))]^2 , \tag{10}$$

where $I_{1,j}(0)$ and $I_{2,j}(0)$, $j = 1, ..., N$, are the initial conditions of a set of N orbits and $I_{1,j}(t)$ and $I_{2,j}(t)$ are the corresponding values at time t. The term in the squared brackets of (10) represents the square of the distances of the actions from the initial values, projected on the resonant line $I_1 = 2I_2$. The estimates of D versus $1/\varepsilon$ are provided in Figure 7 on a logarithmic scale. Clearly, we can exclude a linear regression, which would correspond to a power law $D(\varepsilon) = C\,(1/\varepsilon)^m$. For some different sets of data, we performed local regression, finding different slopes. In particular, the results are the following: the set containing the values of D for $1/\varepsilon \leq 55$ has slope $m = -4.5$; the set for $62 \leq 1/\varepsilon \leq 250$ has $m = -6.9$; the set with $1/\varepsilon \geq 330$ has $m = -8.8$. The changes of the slopes agree with the expected exponential decrease of D. An exponential fit of the form $D(\varepsilon) = C' \exp(-\kappa/\varepsilon)^\alpha$ (for some parameters κ and α) requires a larger ε–range, which is outside our computational possibilities. To give en example, the value of D for $1/\varepsilon = 1000$ (see Figure 7) required 4 months of CPU time on a fast workstation (Compaq AlphaStation XP1000 6/667mhz).

Acknowledgments: One of the authors (A.C.) is deeply indebted to L. Chierchia for useful suggestions and discussions.

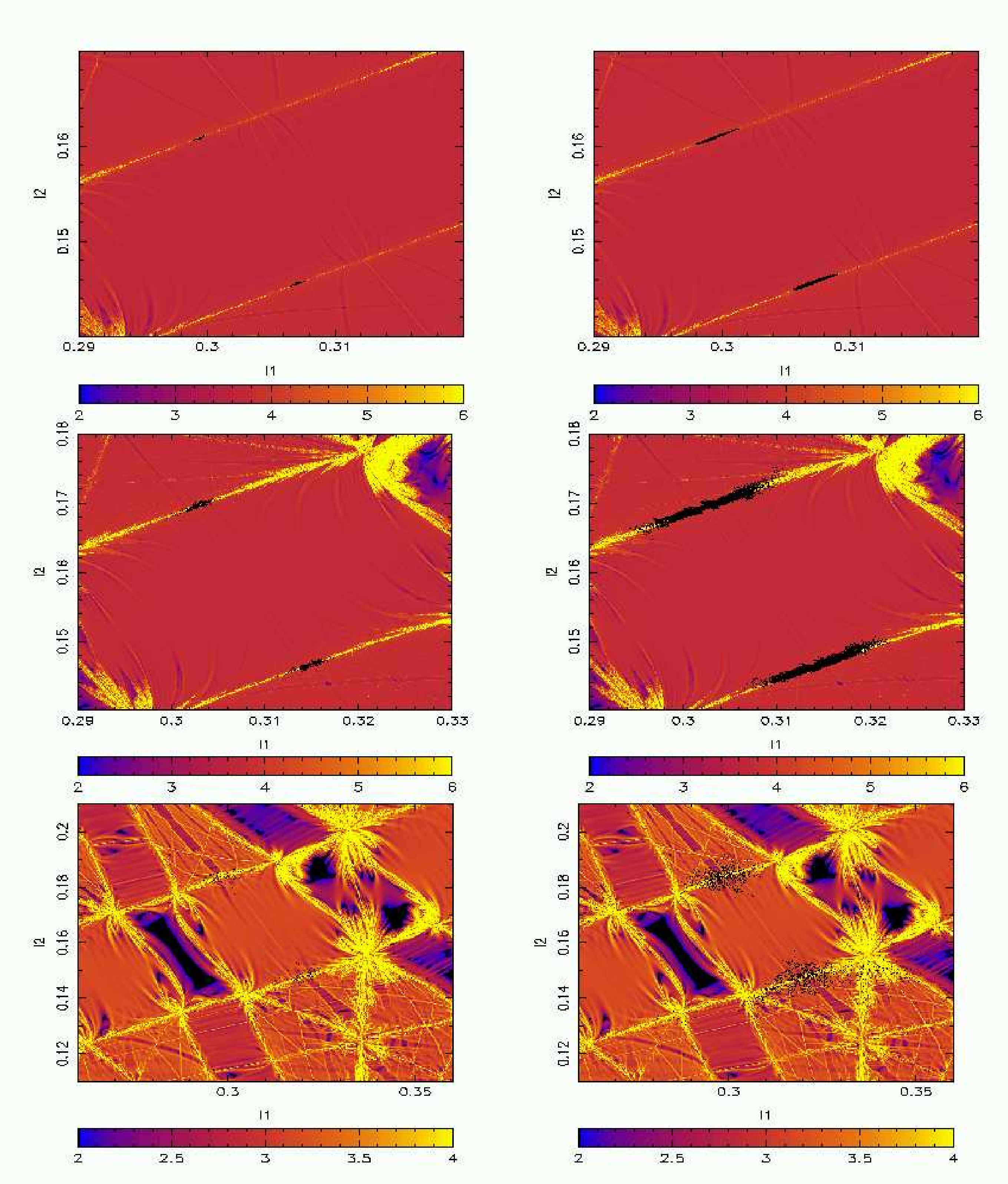

Figure 6: Diffusion along the resonant line $I_1 = 2I_2$ for $\varepsilon = 0.003$ (top), $\varepsilon = 0.007$ (middle), $\varepsilon = 0.02$ (bottom) of a set of 100 initial conditions in the hyperbolic border of the resonance within the interval $0.303 \leq I_1 \leq 0.304$ and $0.143 \leq I_2 \leq 0.144$. Black points correspond to the intersections of the orbits on the double section $|\varphi_1| + |\varphi_2| \leq 0.05$, $\varphi_3 = 0$. The integration times are respectively: 10^7 (top, left), 10^8 (top, right), 10^6 (middle, left), $2.4 \cdot 10^7$ (middle, right), $1.6 \cdot 10^4$ (bottom, left), $5 \cdot 10^5$ (bottom, right). The colour ranges from black to yellow (from [39]).

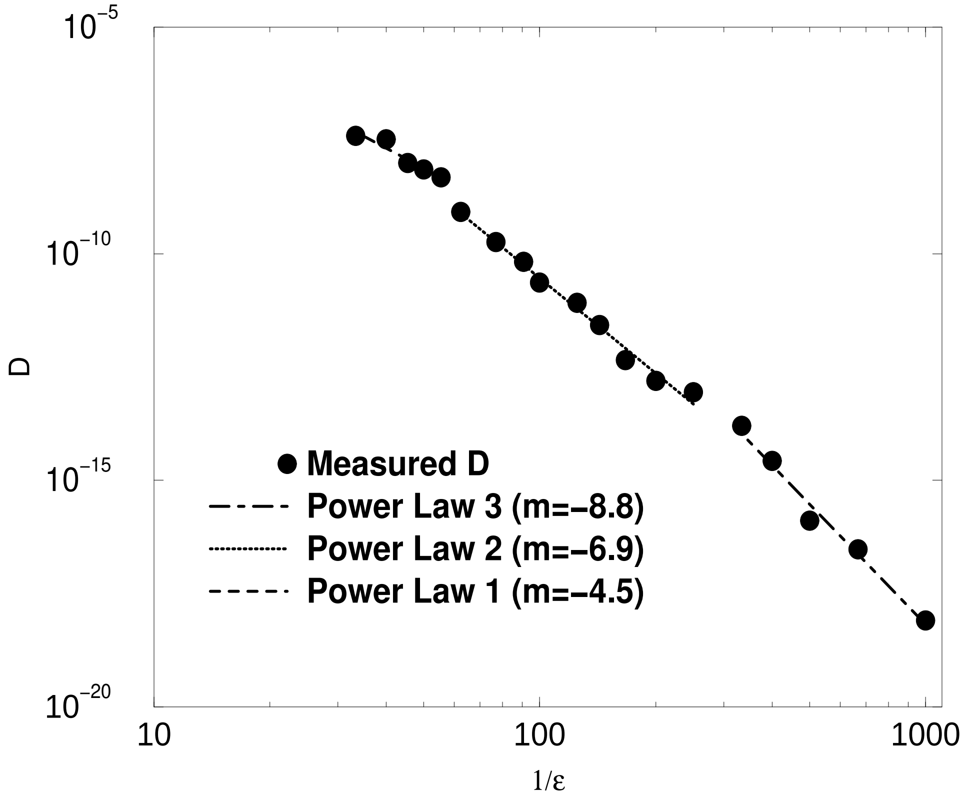

Figure 7: Computation of the diffusion coefficient as a function of $1/\varepsilon$. The change of the slope of the three power–law fits agrees with the expected exponential decrease of D (from [39]).

References

[1] V.I. Arnold. Proof of a Theorem by A.N. Kolmogorov on the invariance of quasi-periodic motions under small perturbations of the Hamiltonian. *Russ. Math. Surveys*, **18**, 9 (1963)

[2] V. I. Arnold. Small denominators and problems of stability of motion in classical and Celestial Mechanics. *Russian Math. Survey*, **18**, 85 (1963)

[3] V.I. Arnold. Instability of dynamical systems with several degrees of freedom. *Sov. Math. Dokl.*, **6**, 581 (1964)

[4] V. I. Arnold. *Mathematical methods of classical mechanics.*, Springer–Verlag, New York (1978) (Russian original, Moscow, 1974)

[5] V. I. Arnold (editor). *Encyclopaedia of Mathematical Sciences.* Dynamical Systems III, Springer-Verlag **3** (1988)

[6] G. Benettin, F. Fassó, M. Guzzo. Nekhoroshev-stability of L_4 and L_5 in the spatial restricted three-body problem. *Regular and Chaotic Dynamics*, **3**, 56 (1988)

[7] G. Benettin, G. Gallavotti. Stability of motions near resonances in quasi integrable Hamiltonian systems. *Journ. Stat. Phys.*, **44**, 293 (1986)

[8] A. Celletti. Analysis of resonances in the spin–orbit problem in Celestial Mechanics: The synchronous resonance (Part I). *J. of Appl. Math. and Phys. (ZAMP)*, **41**, 174 (1990)

[9] A. Celletti, L. Chierchia. Rigorous estimates for a computer-assisted KAM theory. *J. Math. Phys.*, **28**, 2078 (1987)

[10] A. Celletti, L. Chierchia. A Constructive Theory of Lagrangian Tori and Computer–assisted Applications. *Dynamics Reported* (C.K.R.T. Jones, U. Kirchgraber, H.O. Walther Managing Editors), **4** (New Series), Springer–Verlag, 60 (1995)

[11] A. Celletti, L. Chierchia. On the stability of realistic three-body problems. *Commun. Math. Phys.*, **186**, 413 (1997)

[12] A. Celletti, L. Chierchia. *KAM Stability and Celestial Mechanics.* Preprint (2003)

[13] B.V. Chirikov. A universal instability of many dimensional oscillator system. *Phys. Rep.*, **52**, 263 (1979)

[14] G. Contopoulos, N. Voglis. A fast method for distinguishing between order and chaotic orbits. *Astron. Astrophys.*, **317**, 73 (1997)

[15] C. Delaunay. *Théorie du Mouvement de la Lune*. Mémoires de l'Académie des Sciences **1**, Tome XXVIII, Paris (1860)

[16] J.-P. Eckmann, P. Wittwer. *Computer methods and Borel sommability applied to Feigenbaum's equation*. Springer Lecture Notes in Physics, **227** (1985)

[17] C. Falcolini, R. de la Llave. A rigorous partial justification of Greene's criterion. *J. Stat. Phys.*, **67**, n.3/4, 609 (1992)

[18] C. Froeschlé. A numerical study of the stochasticity of dynamical systems with two degrees of freedom. *Astron. Astrophys.*, **9**, 15 (1970)

[19] C. Froeschlé. The Lyapunov characteristic exponents and applications. *Journal de Méc. théor. et appl.*, Numero spécial, 101 (1984)

[20] C. Froeschlé, M. Guzzo, E. Lega. Graphical evolution of the Arnold's web, from order to chaos. *Science*, **289** N.5487, 2108 (2000)

[21] C. Froeschlé, E. Lega. On the measure of the structure around the last KAM torus before and after its break-up. *Celest. Mech. and Dynamical Astron.*, **64**, 21 (1996)

[22] C. Froeschlé, E. Lega. Twist angles, a fast method for distinguishing islands, tori and weak chaotic orbits. Comparison with other methods of analysis. *Astron. Astrophys.*, **334**, 355 (1998)

[23] C. Froeschlé, E. Lega. On the structure of symplectic mappings. The fast Lyapunov indicator, a very sensitive tool. *Celest. Mech. and Dynamical Astronomy*, **78**, 167 (2000)

[24] C. Froeschlé, E. Lega, R. Gonczi. Fast Lyapunov indicators. Application to asteroidal motion. *Celest. Mech. and Dynam. Astron.*, **67**, 41 (1997)

[25] G. Gallavotti. *The Elements of Mechanics*. Springer–Verlag, New York (1983)

[26] J.M. Greene. A method for determining a stochastic transition. *J. of Math. Phys*, **20**, 1183 (1979)

[27] M. Guzzo, E. Lega, C. Froeschlé. On the numerical detection of the stability of chaotic motions in quasi–integrable systems. *Physica D*, **163**, 1 (2002)

[28] M. Guzzo, A. Morbidelli. Construction of a Nekhoroshev like result for the asteroid belt dynamical system. *Cel. Mech. and Dyn. Astron.*, **66**, 255 (1997)

[29] M. Hénon. Explorationes numérique du problème restreint IV: Masses egales, orbites non periodique. *Bullettin Astronomique*, **3**, no. 1, fasc. 2, 49 (1966)

[30] M. Hénon, C. Heiles. The applicability of the third integral of motion: Some numerical experiments. *Astron. J.*, **1**:73 (1964)

[31] H. Koch, A. Schenkel, P. Wittwer. Computer-Assisted Proofs in Analysis and Programming in Logic: A Case Study. *SIAM Review*, **38**, n. 4, 565 (1996)

[32] A.N. Kolmogorov. On the conservation of conditionally periodic motions under small perturbation of the Hamiltonian. *Dokl. Akad. Nauk. SSR*, **98**, 469 (1954)

[33] O.E. Lanford III. Computer assisted proofs in analysis. *Physics A*, **124**, 465 (1984)

[34] J. Laskar. The chaotic motion of the solar system. A numerical estimate of the size of the chaotic zones. *Icarus*, **88**, 266 (1990)

[35] J. Laskar. Frequency analysis for multi-dimensional systems. Global dynamics and diffusion. *Physica D*, **67**, 257 (1993)

[36] J. Laskar. Large scale chaos in the solar system. *Astron. Astrophys.*, **287**, L9 (1994)

[37] J. Laskar, C. Froeschlé, A. Celletti. The measure of chaos by the numerical analysis of the fundamental frequencies. Application to the standard mapping. *Physica D*, **56**, 253 (1992)

[38] E. Lega, C. Froeschlé. *Fast Lyapunov Indicators. Comparison with other chaos indicators. Application to two and four dimensional maps.* In The Dynamical Behaviour of Our Planetary System. Kluwer academ. publ., J. Henrard and R. Dvorak eds. (1997)

[39] E. Lega, M. Guzzo, C. Froeschlé. Detection of Arnold diffusion in Hamiltonian systems. *Physica D*, accepted (2003)

[40] A.J. Lichtenberg, M.A. Lieberman. *Regular and Stochastic motion.* Springer, Berlin, Heidelberg, New York (1983)

[41] P. Lochak. On the conservation of conditionally periodic motions under small perturbation of the Hamiltonian. *Russ. Math. Surv.*, **47**, 57 (1992)

[42] R.S. MacKay. Greene's residue criterion. *Nonlinearity*, **5**, 161 (1992)

[43] M. Month, J.C.Herrera. *Nonlinear dynamics and the beam-beam interaction.* American Institute of Physics, Month and Errera eds. (1979)

[44] J. Moser. On invariant curves of area-preserving mappings of an annulus. *Nach. Akad. Wiss. Göttingen, Math. Phys. Kl. II*, **1**, 1 (1962)

[45] N.N. Nekhoroshev. Exponential estimates of the stability time of near-integrable Hamiltonian systems. *Russ. Math. Surveys*, **32**, 1 (1977)

[46] D. Nesvorny, S. Ferraz-Mello. On the asteroidal population of the first-order Jovian resonances. *Icarus*, **130**, 247 (1997)

[47] Y. Papaphilippou, J. Laskar. Global dynamics of triaxial galactic models through frequency map analysis. *Astronomy and Astrophysics*, **329**, 451 (1998)

[48] H. Poincaré. *Les méthodes nouvelles de la méchanique céleste.* Gauthier Villars, Paris (1899)

[49] J. Pöschel. Nekhoroshev's estimates for quasi-convex Hamiltonian systems. *Math. Z.*, **213**, 187 (1993)

[50] C.L. Siegel, J.K. Moser. *Lectures on Celestial Mechanics.* Springer–Verlag Berlin Heidelberg, New York (1971)

[51] V. Szebehely. *Theory of orbits.* Academic Press, New York and London (1967)